# Optical Test Set for Microwave Fiber-Optic Network Analysis

DAVID D. CURTIS, MEMBER, IEEE, AND ELIZABETH E. AMES, MEMBER, IEEE

*Abstract*—An optical test set is presented which can be used with any vector network analyzer for measuring microwave transmission and reflection scattering parameters of fiber-optic components. Measurement configurations and operating characteristics are discussed. Calibration of the network analyzer, which is performed using fiber-optic offset shorts, matched load, and thru calibration standards, is discussed, reflection error terms are computed, and de-embedding relations are given for transmission and reflection measurements. A frequency response normalization is also presented as an alternative means of de-embedding reflection magnitude and phase. Accuracy limitations are addressed in terms of connector repeatability, calibration repeatability, accuracy of the calibration standards, test set dynamic range, and resolution. $S$ matrices measured at 2.0 GHz are also presented to illustrate the utility of characterizing fiber-optic components in terms of microwave performance when designing a microwave fiber-optic network.

## I. Introduction

THE USE OF lightwave technology is becoming increasingly popular in antenna remoting links [1] and in prototype true time delay signal processing applications such as optical beam-forming networks for array antennas [2]–[4] and matched filters [5]. While the electrical scattering parameters of these networks are easily measured using a vector network analyzer, this type of characterization is strictly external. To facilitate the design of these networks it is desirable to evaluate the microwave performance of the fiber-optic components within the network, which requires a means of interfacing a network analyzer with the microwave signals that reside in the optical regime as intensity modulation of the lightwave carrier. Development of a network analyzer tailored for this purpose has been reported [6] and is commercially available [7]. However, theoretical aspects related to network analyzer calibration and de-embedding techniques for optical regime measurement of microwave signals have not been reported in the literature. Issues pertaining to measurement accuracy and repeatability have not been addressed; nor have definitions been given for microwave scattering parameters of optical components.

In this paper we introduce an optical test set (OTS) complete with fiber-optic calibration standards, which follows the convention of using a thru standard for transmission calibration, and two offset shorts and a matched load for reflection calibration. The reflection error correction terms used in this technique are determined from calculated and measured reflection scattering parameters of the offset shorts and matched load calibration standards. De-embedding relations are given for transmission and reflection measurements. A normalization technique using the frequency response tracking error term is also presented as a simplified reflection de-embedding method. Calibration of the network analyzer and scattering parameter measurements are made directly in the optical regime by tracking the microwave intensity envelope of the lightwave carrier. The measurement uncertainty of the OTS is determined from the repeatability of connections and calibration standards, comparison of calculated versus measured $S$ parameters of the calibration standards, and measurements of known fiber-optic attenuators and cleaved fiber. OTS dynamic range and resolution are also given, based on experimental results. We present scattering matrices of a fiber-optic directional coupler, a $1\times2$ switch, and a true time delay network composed of these components, measured at 2.0 GHz.

We begin this paper with definitions of the microwave scattering parameters of optical components in terms of lightwave modulation wave variables. The optical standing wave ratio is introduced, and relations are given for the fiber-optic $S$ parameters in terms the electrical power ratios displayed by the network analyzer.

## II. $S$-Parameter Characterization of Microwave Fiber-Optic Networks

The two-port black box illustrated in Fig. 1 is representative of the RF wave behavior measured between any two ports of a microwave fiber-optic network. Parameters $S^E_{nm}$ and $S^E_{nn}$ are the commonly known electrical scattering parameters, measured using a conventional network analyzer. Internal to the two-port black box are lightwave transducers that modulate and demodulate the microwave signal upon the optical carrier wave. A commonly used method of optical carrier modulation and demodulation is depicted in Fig. 2 to facilitate the definitions of the modulation scattering parameters, $S^o_{nm}$ and $S^o_{nn}$, which follow. In Fig. 2, a microwave signal is impressed upon the lightwave carrier as double-sideband intensity modulation. This is readily accomplished by direct modulation of the bias

Manuscript received August 21, 1989; revised December 3, 1989. This work was supported by the Department of the Air Force.

D. D. Curtis is with the Antenna Technology Branch, Electromagnetics Directorate, Rome Air Development Center, Hanscom AFB, MA 01731.

E. E. Ames is with the Department of Electrical and Computer Engineering, Northeastern University, Boston, MA 02115.

IEEE Log Number 9034629.

0018-9480/90/0500-0552$01.00 

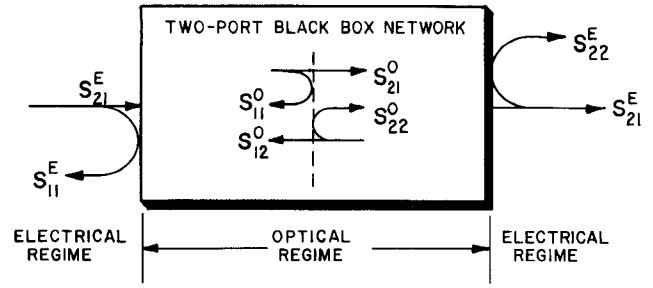


Fig. 1. Microwave fiber-optic two-port black box network representing the external electrical scattering parameters and internal fiber-optic scattering parameters.

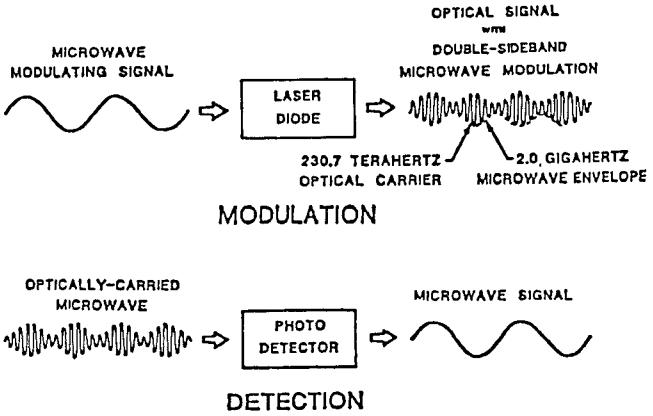


Fig. 2. Modulation and demodulation of an optically carried microwave by means of direct laser diode modulation and p-i-n photodiode detection.

current applied to the optical source, a semiconductor laser diode. Demodulation is performed by a reverse-biased photodiode, an optical detector that produces an RF current as the square of the detected optical carrier electric field. In both the modulation and demodulation processes, microwave current is linear with the envelope of the optical intensity.

### A. Definition of $S^o_{nn}$ and $S^o_{nm}$

Since the microwave signal resides on the optical carrier as an intensity envelope, it is subject to the same optical regime phenomena as the carrier. These effects include modal, material, and waveguide dispersion [8], scattering [9], and optical reflections from discontinuities that are on the order of the optical wavelength. Measurements made in the optical regime are in fact measurements of the microwave envelope, not the carrier wave. We define wave variables $a^o_n$ and $b^o_n$ for the incident and emergent optical power waves, respectively, which occur at the $n$th port within the fiber-optic network. The incident wave at the $n$th port is given as

$$a^o_n = \Phi_{an} M \cos(\omega_M t + \phi^o_{an}) \tag{1}$$

where $\Phi_{an}$ is the incident average optical power, $M$ is the modulation index, $\omega_M$ is the RF modulation angular frequency, and $\phi^o_{an}$ is the incident RF phase angle. Similarly, the emergent wave variable from the $n$th port can be defined as

$$b^o_n = \Phi_{bn} M \cos(\omega_M t + \phi^o_{bn}) \tag{2}$$

where $\Phi_{bn}$ is the emergent average optical power and $\phi^o_{bn}$ is the emergent RF phase angle. Transforming (1) and (2) to phasors with $\cos \omega_M t$ as the reference and following the definition of electrical scattering parameters [10], we obtain the reflection scattering parameter at the $n$th fiber-optic port:

$$S^o_{nn} = \frac{b^o_n}{a^o_n} = \frac{\Phi_{bn}}{\Phi_{an}} e^{-j(\phi^o_{bn} - \phi^o_{an})}. \tag{3}$$

The magnitude of $S^o_{nn}$ yields the reflection coefficient, $\Gamma_o = \Phi_{bn}/\Phi_{an}$, from which the optical return loss is obtained as $10 \log |\Gamma_o|$. Reflection RF phase is obtained directly from (3) as $\phi^o_{nn} = \phi^o_{bn} - \phi^o_{an}$.

By introducing a second set of wave variables similar in form to (1) and (2), corresponding to the $m$th fiber-optic port, we obtain the forward transmission scattering parameter:

$$S^o_{nm} = \frac{b^o_n}{a^o_m} = \frac{\Phi_{bn}}{\Phi_{am}} e^{-j(\phi^o_{bn} - \phi^o_{am})}. \tag{4}$$

The magnitude of $S^o_{nm}$ is the transmission coefficient, $T_o = \Phi_{bn}/\Phi_{am}$, from which the insertion loss of the optical path from port $m$ to port $n$ is obtained as $10 \log |T_o|$. The RF insertion phase, $\phi^o_{nm} = \phi^o_{bn} - \phi^o_{am}$, is obtained directly from (4). By substituting $m$ for $n$, and visa versa, (4) becomes the reverse transmission scattering parameter, $S^o_{mn}$.

### B. Optical Standing Wave Ratio

Discontinuities in the optical path give rise to reflections of the optical carrier and subsequently the microwave envelope. As a result, an optical intensity standing wave is formed with microwave periodicity due to the superposition of the forward and reverse traveling microwave envelopes. The optical standing wave ratio, $OSWR$, is then given as

$$OSWR = \frac{1 + |\Gamma_o|}{1 - |\Gamma_o|} \tag{5}$$

which can be used as a figure of merit for optical components used in microwave fiber-optic networks.

### C. Measuring $S^o_{nn}$ and $S^o_{nm}$ in Terms of Electrical Wave Variables

Since the measured data obtained from the network analyzer involve a comparison of electrical wave variables, $a^E_n$ and $b^E_n$, defined in [10], conversion relations between the electrical and optical wave variables are required for a meaningful interpretation of fiber-optic component performance. The required conversion relations can be derived from the interaction of electrical current and optical power at the laser and the photodiode.

Direct modulation of a laser diode is a linear operation provided that the laser bias current and RF modulation index are adjusted in such a way that the peak-to-peak excursion of the RF-modulated bias current is between the

threshold current and the −1 dB compression point of the laser [8]. Assuming these conditions are met, the linear relation for the microwave envelope of the optical power, $a_n^o$, versus the microwave modulating current, $a_n^E$, that is produced by the network analyzer is given by

$$|a_n^o|e^{-j\phi_{an}^o} = \eta|a_n^E|e^{-j\phi_{an}^E} \tag{6}$$

where $\eta$ is the slope of the optical power versus electrical current characteristic for the laser diode. Equation (6) is not a valid expression over a modulation bandwidth because the modulation response, $\Phi(f_{RF})/i(f_{RF})$, is a nonlinear function of the modulating RF frequency, $f_{RF}$ [11]. However, the nonlinear response of the laser is removed from the measured data during de-embedding.

Demodulation of the optically carried microwave by a p-i-n photodiode obeys the following square-law relation [12]:

$$i = R(\lambda)|E|^2 \tag{7}$$

where $i$ is the generated photocurrent, and $R(\lambda)$ is the spectral responsivity, which reduces to $R_\lambda$ for a single-mode fiber network. $R_\lambda$ is valid for RF-modulated optical signals since the modulating frequency is four to five orders of magnitude lower than the frequency of the optical carrier. Substitution of $|b_n^o| = \Phi_{bn} = |E|^2$ and $b_n^E = i$ in (7) and accounting for the phase of the RF signal, we obtain a linear relation between the optical power wave, $b_n^o$, and the photocurrent, $b_n^E$, received by the network analyzer:

$$|b_n^E|e^{-j\phi_{bn}^E} = R_\lambda|b_n^o|e^{-j\phi_{bn}^o}. \tag{8}$$

Combining (6) and (8), we obtain

$$\frac{|b_n^E|}{|a_n^E|}e^{-j(\phi_{bn}^E-\phi_{an}^E)} = R_\lambda\eta\frac{|b_n^o|}{|a_n^o|}e^{-j(\phi_{bn}^o-\phi_{an}^o)} \tag{9}$$

where the left side of (9) is $S_{nn}^E$ and the right side is $R_\lambda\eta S_{nn}^o$. However, since electrical scattering parameters are displayed by the network analyzer as power ratios and since $a_n^E$ and $b_n^E$ are microwave currents, both sides of (9) must be squared, which produces the following equation:

$$S_{nn}^E = (R_\lambda\eta)^2|S_{nn}^o|^2e^{-j\phi_{nn}^o}. \tag{10}$$

Upon de-embedding, the coefficient $(R_\lambda\eta)^2$ will be removed; therefore, we write the following conversion relation between $S_{nn}^E$ and $S_{nn}^o$:

$$S_{nn}^E = |S_{nn}^o|^2e^{-j\phi_{nn}^o} \tag{11}$$

from which the electrical return loss displayed by the network analyzer is related to the optical return loss of the device under test (DUT) as

$$|\Gamma_E| = |\Gamma_o|^2. \tag{12}$$

When measurements are displayed on a log scale, (11) and (12) become, respectively,

$$S_{nn}^E = 2|S_{nn}^o|e^{-j\phi_{nn}} \tag{13}$$

$$|\Gamma_E| = 2|\Gamma_o|. \tag{14}$$

By substituting transmission wave variables for reflection wave variables in (9), the following conversion relations are obtained for the forward transmission scattering parameter and insertion loss, for linear and log scales, respectively:

$$S_{nm}^E = |S_{nm}^o|^2e^{-j\phi_{nm}^o} \tag{15}$$

$$|T_E| = |T_o|^2 \tag{16}$$

$$S_{nm}^E = 2|S_{nm}^o|e^{-j\phi_{nm}^o} \tag{17}$$

$$|T_E| = 2|T_o|. \tag{18}$$

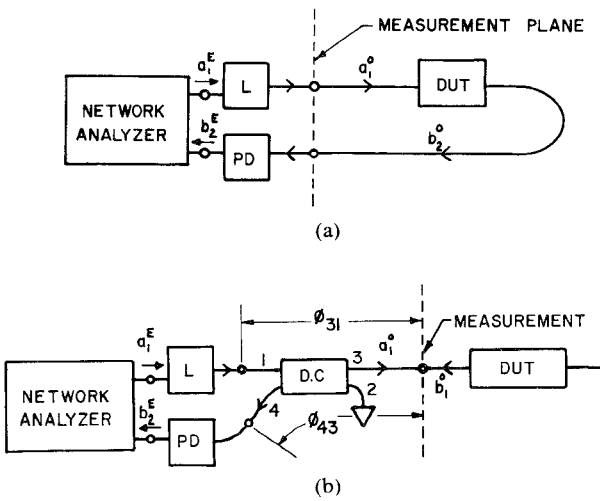


Fig. 3. (a) OTS transmission scattering parameter measurement configuration. (b) OTS reflection scattering parameter measurement configuration with frequency response tracking normalization path lengths indicated relative to the measurement plane. Triangles indicate optical matched loads used to suppress reflections during measurement.

## III. Optical Test Set Operation

The optical test set fabricated for this experiment features an InGaAsP buried crescent laser diode which emits near-infrared light at a wavelength of 1286.4 nm, corresponding to an optical frequency of approximately 230.7 THz. In all calibration and device measurements, the laser was biased at 40 mA and the RF modulation was 0.0 dBm, corresponding to a 0.45 modulation index. The laser impedance, approximately 3 Ω, is matched to 50 Ω using a 47 Ω discrete resistor. The photodiode is an InGaAsP p-i-n device with a responsivity $R_\lambda = 0.6$ at the 1300 nm optical wavelength. The photodiode is reverse-biased at −10 V, its impedance is approximately 1500 Ω, and the device is impedance matched to 50 Ω using a shunt resistor. Both the laser and the photodiode were purchased with step-index single-mode fiber pigtails. The fiber core diameter is 8.7 μm, and the cladding diameter is 125 μm. The effective refractive index of the fiber is 1.4642 and the fiber attenuation is rated at 0.5 dB/km.

### A. Measurement Configurations

The OTS is shown in the $S_{nm}^o$ transmission measurement configuration in Fig. 3(a). The network analyzer operates in the $S_{21}^E$ mode, providing microwave modulation, $a_1^E$, to the laser from port 1 of the network analyzer's electrical

test set. The optically carried microwave, $a_1^o$, propagates from the laser and is incident upon the DUT. The optical signal emergent from the DUT, $b_2^o$, propagates to the photodiode, where it is demodulated to an electric current, $b_2^E$, that returns to port 2 of the network analyzer. This measurement configuration is used for forward and reverse transmission scattering parameters; however, the DUT must be oriented backwards when measuring $S_{mn}^o$.

The OTS is shown in the $S_{nn}^o$ reflection measurement configuration in Fig. 3(b). The network analyzer operates in the $S_{21}^E$ mode, as it does for transmission scattering parameter measurements with the reflected signal returning to port 2 of the network analyzer, since the electro-optic isolation of the laser prevents single port measurements of $S_{nn}^o$. As in the $S_{nm}^o$ case, the microwave signal emerging from port 1 of the network analyzer modulates the laser diode, and the optically carried microwave propagates through a $-3$ dB fiber-optic directional coupler to the DUT. The reflected signal, which is measured with respect to the reflection measurement plane, shown in Fig. 3(b), is split by the $-3$ dB coupler, causing slightly less than half of the reflected signal to reach the photodiode due to the 0.522 thru- and 0.478 cross-coupling coefficients and the 0.01% excess loss of the directional coupler used in our optical test set.

### B. Calibration and De-embedding

*1) Transmission Calibration Using a Fiber-Optic Thru Calibration Standard:* Calibration of the network analyzer for transmission measurements is accomplished using a short length of fiber as a thru calibration standard inserted in the $S_{nm}^o$ configuration in place of the DUT. Calibration data are recorded and since the network analyzer operates in the $S_{21}^E$ mode, the actual scattering parameter of the DUT is de-embedded from the measured data automatically according to the following relation:

$$S_{nm}^E = \frac{S_{nm}^E}{S_{nm}^{\text{cal}}} \tag{19}$$

where $S_{nm}^{\text{cal}}$ is the nonlinear frequency response of the laser with the photodiode, as described in subsection II-C.

*2) Reflection Calibration Using Fiber-Optic Offset Shorts, and Matched Load Calibration Standards:* Since reflection measurements are made with the network analyzer operating in the $S_{21}^E$ mode, the network analyzer is not programmed for a reflection calibration and it will not de-embed $S_{nn}^o$ automatically. Instead, a separate reflection measurement is made for each of the three reflection calibration standards, and the measured data are used to de-embed the actual reflection scattering parameter using a calculator or a computer.

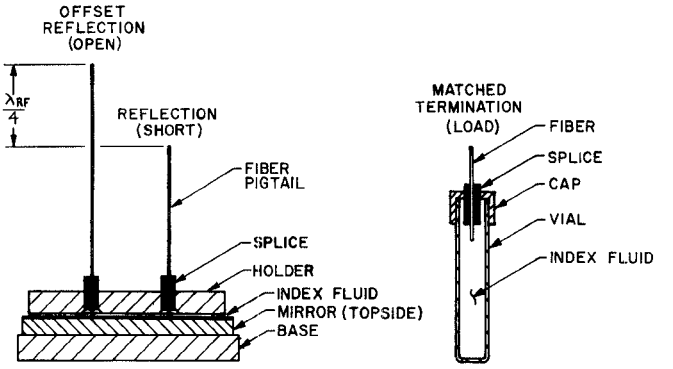


Fig. 4. Cross-sectional diagram of the two offset shorts and matched load reflection calibration standards.

The offset shorts and matched load reflection calibration standards are shown in Fig. 4. The optical matched load consists of a single-mode fiber pigtail terminated in a vial of refractive index matching gel. Several matched loads were fabricated and they exhibited an average optical return loss of approximately $-50$ dB. The offset shorts were fabricated by terminating two cleaved fibers normal to a mirror. The length of the fiber pigtail is arbitrary for the first short, but the pigtail length of the offset short is 90° longer than the first, approximately 2.56 cm at 2.0 GHz. The round-trip path length offset is 180° at 2.0 GHz, giving the offset short the appearance of an open circuit to the microwave modulation. An additional 90° offset was added to both shorts to simplify their fabrication.

De-embedding the actual reflection coefficient, $S_{nn}^o$, from the measured value, $S_{nn}^E$, is accomplished by calculating the error terms which are defined in terms of parameters $a$, $b$, and $c$ [13]:

$$E_{01}E_{10} = a - bc \qquad \text{frequency response tracking error term} \tag{20}$$

$$E_{00} = b \qquad \text{directivity error term} \tag{21}$$

$$E_{11} = -c \qquad \text{load match error term.} \tag{22}$$

The parameters $a$, $b$, and $c$ are calculated from the following three equations [13], which contain $A_i$, the calculated complex reflection coefficients of the offset shorts and matched load, and $M_i$, the measured complex reflection coefficients of the three standards:

$$a = \frac{M_1M_2(A_2 - A_1) + M_2M_3(A_3 - A_2) + M_3M_1(A_1 - A_3)}{A_1M_1(A_3 - A_2) + A_2M_2(A_1 - A_3) + A_3M_3(A_2 - A_1)} \tag{23a}$$

$$b = \frac{M_1M_2A_3(A_1 - A_2) + M_2M_3A_1(A_2 - A_3) + M_3M_1A_2(A_3 - A_1)}{A_1M_1(A_3 - A_2) + A_2M_2(A_1 - A_3) + A_3M_3(A_2 - A_1)} \tag{23b}$$

$$c = \frac{A_1(M_3 - M_2) + A_2(M_1 - M_3) + A_3(M_2 - M_1)}{A_1M_1(A_3 - A_2) + A_2M_2(A_1 - A_3) + A_3M_3(A_2 - A_1)} \tag{23c}$$

TABLE I
CALCULATED REFLECTION COEFFICIENTS ($A_i$) VERSUS MEASURED ($M_i$) FOR THE FIBER-OPTIC OFFSET SHORTS AND MATCHED LOAD REFLECTION CALIBRATION STANDARDS: DE-EMBEDDED $M_i$ VERSUS IDEAL SHORT, OPEN, AND LOAD

| Cal. Std. | $A_i$ | $M_i$ measured | $M_i$ de-embedded | Ideal |
|---|---|---|---|---|
| SHORT | -0.9374 - j0.0327 | -0.0194 - j0.0436 | -0.9513 + j0 | -1 + j0 |
| OFFSET | 0.8502 + j0.0148 | 0.0146 + j0.0380 | 0.8108 + j0.0425 | 1 + j0 |
| LOAD | $10^{-6}$ + j0.0320 | (noise floor) | --- | 0 + j0 |

Data obtained for $M_i$ by measurement and $A_i$ by calculation are shown in Table I for comparison with the case of an ideal short, open, load. The measured $M_i$ are the electrical values displayed by the network analyzer. $M_i$ were measured using the OTS configured for $S^o_{nn}$, yet the measurements are relative only to an $S^o_{nm}$ thru calibration of the laser and photodiode. Therefore, the $M_i$ include insertion loss and path length of the directional coupler and the connecting splices, whereas $A_i$ do not include these factors. In subsection C, we will show that, after de-embedding, the $M_i$ are in very close agreement with the calculated $A_i$ and the ideal values for the short, open, and load. The de-embedded values for $M_i$ are shown in the third column of Table I. Several sets of offset shorts and matched loads were fabricated and tested. The data listed in Table I were selected from one such set and are typical for these components at the single frequency point, 2.0 GHz.

Equations (23a)–(23c) are computed, and the resulting values of $E_{01}E_{10}$, $E_{00}$, and $E_{11}$ are substituted into the following de-embedding relation for each measurement frequency [13]:

$$S^o_{nn} = \frac{S^E_{nn} - E_{00}}{E_{01}E_{10} + E_{11}\left(S^E_{nn} - E_{00}\right)}. \tag{24}$$

The magnitudes of $A_i$ were calculated using

$$|\Gamma_o| = \frac{P_r}{P_i} \tag{25}$$

where $P_i$ is the optical power incident upon the calibration standard, measured using an optical power meter at the reflection measurement reference plane prior to connecting the calibration standard. $P_r$ is the reflected power, which is obtained by subtracting the path losses of the $S_{43}$ path through the directional coupler from the output power measured at port 4 of the directional coupler. The phases of $A_i$ were determined by measuring the pigtail fiber of each calibration standard using the OTS in the $S^o_{nm}$ configuration in which each pigtail was, in turn, the DUT. The magnitudes of the offset shorts are fairly high. The phase difference between the short and offset short is 181° at 2.0 GHz for the round-trip of the incident and reflected waves. The phase difference between the short and load is 1° at 2.0 GHz. Ideally these values should be 180° and 0°, respectively, since the offset short is $\lambda/4$ longer than the short and the load is in the same plane as the short. Finally, the following de-embedding relation is obtained for our OTS at the measurement frequency of 2.0 GHz when the computed error terms are substituted into (24):

$$S^o_{nn} = \frac{S^E_{nn}}{(0.0185 + j0.0457) + (-0.0343 + j0.0384)\,S^E_{nn}}. \tag{26}$$

*3) Frequency Response Tracking Normalization Technique:* In most of the reflection measurements made using the OTS, the magnitudes of the reflection coefficients were $-20$ dB or less, indicating good refractive index match. In (24), the directivity error term, $E_{00}$, was below the system noise floor, due to the 50 dB directivity of the directional coupler. Since $E_{00}$ is negligible, a frequency normalization can be used to de-embed reflection coefficient data when $E_{11}$ in (24) is small so that

$$E_{11}S^E_{nn} \ll E_{01}E_{10}. \tag{27}$$

Given this condition, the de-embedding relation in (24) simplifies to the following approximation:

$$S^A_{nn} \approx \frac{S^M_{nn}}{E_{01}E_{10}} \tag{28}$$

where the measured data are normalized by the frequency response tracking error term, $E_{01}E_{10}$, to obtain the actual reflection scattering parameter of the DUT. Further, one does not need to compute the parameters $a$, $b$, and $c$ obtained using the offset shorts and matched load. Instead, the forward $S_{31}$ path and the reflection $S_{43}$ path of the directional coupler, shown in Fig. 3(b), are inserted, in turn, into the OTS configured for $S^o_{nm}$ measurements. In this way, the frequency response of the forward and reflected paths through the directional coupler is measured and de-embedded automatically by the $S^o_{nm}$ calibration. Provided the lengths of the forward and reflected paths do not change, the $E_{01}E_{10}$ error term must be measured only once. For our OTS at 2.0 GHz, we obtained the following frequency normalization de-embedding relations for the magnitude, in optical power dB, and phase, in degrees:

$$|S^o_{nn}| = (1/2)\left(|S^E_{nn}| + 13.0\text{ dB}\right) \tag{29}$$

$$\phi^o_{nn} = \phi^E_{nn} - 66°. \tag{30}$$

TABLE II
OPTICAL TEST SET PERFORMANCE AT 2.0 GHz WHEN USED WITH AN HP8510B NETWORK ANALYZER: $S^o_{nn}$ DATA ARE FOR OFFSET SHORTS/LOAD CALIBRATION

| | Magnitude | | | Phase | |
|---|---|---|---|---|---|
| | Dynamic Range | Uncertainty | Resolution | Uncertainty | Resolution |
| $S^o_{nm}$ | 47.4 dB | ± 0.15 dB | 0.001 dB | ± 1° | ± 0.001° |
| $S^o_{nn}$ | 40.9 dB | ± 0.15 dB | 0.001 dB | ± 2° | ± 0.001° |

### C. Repeatability of Reflection Calibration Standards

The accuracy of the OTS is dependent upon connection repeatability, calibration repeatability, and the accuracy of the error correction terms. In this subsection, we will address these issues, beginning with connector repeatability. Elastomeric splices were used in all fiber-to-fiber connections. When new, the splices exhibited a 0.2 dB optical insertion loss, but after repeated usage the splice loss became random. The mean insertion loss was 0.36 dB with a 0.15 standard deviation, measured over 60 trials. Thus, during extended use of the OTS, measurement uncertainty due to splice repeatability is $\pm 0.15$ dB optically, or $\pm 0.30$ dB electrically. In all cases, the splices exhibited zero RF insertion phase.

Repeatability of the reflection calibration standards was determined from the $M_t$ calibration data taken during several $S^o_{nn}$ measurement sessions using the same offset shorts and matched load. For both the short and offset short, the magnitude of the optical reflection coefficient ranged between 0.835 and 0.941; however, the reflected RF phases remained constant over the same experimentation period. The magnitude and phase of the matched load were below the OTS noise floor.

The accuracy of the error terms is critical in the offset shorts/load technique. To determine this accuracy limit we de-embedded the measured $M_t$ data using the frequency response tracking normalization technique and compared the results to the calculated $A_t$ values listed in Table I. We recognize that this is not an exact comparison since the de-embedded $M_t$ data are subject to any errors associated with the normalization technique; however, both reflection calibration techniques produced very similar results in all cases where the reflection coefficient data were above the noise floor. For instance, in the case of a cleaved fiber we obtained $S^o_{nn} = -14.44$ dB$\angle 3°$ using the offset shorts/load calibration, whereas the normalization produced $S^o_{nn} = -14.65$ dB$\angle 2°$.

As a further means of comparing the two reflection calibration techniques, we obtained $E_{10}E_{01} = -13.073$ dB$\angle 68°$ using the offset shorts/load technique. This is in very close agreement with the measured average obtained from the normalization technique, $-13.0$ dB$\angle 66°$, given by (30) and (31). Therefore, the de-embedded $M_t$ data listed in Table I are probably very close to the actual scattering parameters of the calibration standards. Upon converting the $A_i$ and de-embedded $M_t$ to magnitude in dB, and phase in degrees, the de-embedded $M_i$ differed from $A_t$ by less than 0.2 dB and 2° at 2.0 GHz. Therefore, we are confident that the error term values in (26) are accurate to this extent.

### D. Resolution, Dynamic Range, and Measurement Uncertainty

The dynamic range, measurement uncertainty, and resolution of our optical test set are summarized in Table II for measurements made at 2.0 GHz made using the OTS with an HP8510B network analyzer. The resolution of the OTS is due entirely to the network analyzer. The dynamic range was determined for $S^o_{nm}$ measurements by calibrating the network analyzer using the fiber-optic thru calibration standard. The network analyzer was then disconnected from the OTS and the electrical noise floor measured $-106.570$ dB from the calibrated value at 2.0 GHz. The photodiode was then connected to port 2 of the network analyzer's electrical test set, and the noise floor rose to $-94.777$ dB. Due to square-law detection, the $S^o_{nm}$ dynamic range of the OTS in dB of optical power is then approximately $-47.4$ dB, relative to a 0 dB reference. The dynamic range of $S^o_{nn}$ measurements is found by substituting the $S^E_{nm}$ dynamic range for $|S^E_{nn}|$ into (29), which yields a $S^o_{nn}$ dynamic range of $-40.9$ dB, relative to 0 dB.

The magnitude uncertainty of $S^o_{nm}$ measurements was determined using attenuators which ranged from $-3$ to $-48$ dB as DUT's in the OTS. The $S^o_{nm}$ magnitude measurements were accurate to within $\pm 0.15$ dB optical power due to the splice loss uncertainty. The phase uncertainty of $S^o_{nm}$ measurements was limited to $\pm 1°$, which was determined by measuring segments of fiber up to 20 RF wavelengths using a millimeter scale and comparing the calculated electrical length of the fiber to the data measured using the OTS.

For $S^o_{nn}$ measurements, the magnitude uncertainty was determined using a single known reference since nearly all of the fiber-optic components measured had return losses below the $-40.9$ dB optical power noise floor of the OTS. As a reference, we calculated the return loss of a cleaved step-index single-mode fiber terminated in air, and then measured its reflection coefficient magnitude using the OTS. Using the effective refractive index of the fiber, $n_{\text{eff}} = 1.4642$, the theoretical reflectivity of the cleaved fiber in air is 3.5%, corresponding to a return loss of $-14.56$ dB. The measured return loss was de-embedded using (26) and we obtained $|\Gamma_o| = -14.44$ dB and $\phi^o_{nn} = 3°$ at 2.0 GHz. The de-embedded phase data are correct to within 2° and the magnitude differed from the calculated value by 0.12 dB.

## IV. Measured Components

### A. Fused Biconical Taper Directional Coupler

Several single-mode fused biconical taper directional couplers were measured using the OTS. The thru- and cross-coupling coefficients ranged from 0.45 to 0.55, with excess losses ranging from 0.01 dB to 0.47 dB. One device in particular was chosen for this discussion because it featured thru- and cross-coupling coefficients of 0.5, with an excess loss of 0.164 dB. The coupling symmetry of this device is useful because at 2.0 GHz the measured scattering matrix below reveals reciprocity upon inspection:

$$S=\begin{bmatrix} 0 & 0.495e^{j231^\circ} & 0.473e^{j78^\circ} & 0 \\ 0.490e^{j230^\circ} & 0 & 0 & 0.495e^{j250^\circ} \\ 0.468e^{j76^\circ} & 0 & 0 & 0.467e^{j95^\circ} \\ 0 & 0.490e^{j251^\circ} & 0.467e^{j95^\circ} & 0 \end{bmatrix}. \tag{31}$$

The manufacturer specified the directivity of this coupler at $-50$ dB, as evident by the off-diagonal zeros in the matrix, which indicate data measured at or below the $-47.4$ dB noise floor of $S^o_{nm}$ measurements. Since the coupler exhibits directivity, this four-port is by definition [10] a sum-and-difference hybrid coupler, with respect to the optical wavelength. It is clear from the matrix above, however, that the directional coupler is simply a power divider with respect to the microwave envelope. The zeros along the main diagonal in the matrix indicate return losses higher than the $-40.9$ dB $S^o_{nn}$ noise floor of the optical test set.

### B. Electromechanical Switch

The scattering matrix given below was obtained from $S$-parameter measurements at 2.0 GHz of a $1\times2$ single-mode fiber-optic switch that is controlled by TTL logic voltages:

$$S=\begin{bmatrix} 0.01e^{j2^\circ} & 0.310e^{j170^\circ} & 0 \\ 0.302e^{j171^\circ} & 0.01e^{-j1^\circ} & 0 \\ 0 & 0 & 0.01e^{j1^\circ} \end{bmatrix}. \tag{32}$$

The switch is reciprocal and the manufacturer's specifications list a 60 dB optical isolation between output ports. As evident by the $S$ matrix, the switch exhibits a 0.01 dB optical reflection coefficient at each port, resulting in an OSWR $=1.020$. The reflection phases measured very close to 0°, as expected, since the pigtail fibers at each port were trimmed to an integer number of RF wavelengths at 2.0 GHz. The given $S$ matrix was measured for the $+5$ V biased output state. Values comparable to the $S^o_{21}$ and $S^o_{12}$ transmission coefficients were measured for $S^o_{31}$ and $S^o_{13}$, and with zeros at $S^o_{21}$ and $S^o_{12}$, for the $S$ matrix of the 0 V output state. Values measured at the OTS noise floor are again represented by zeros, corresponding to the high isolation between output ports.

### C. Switched True Time Delay Network

The fiber-optic network illustrated in Fig. 5 represents a fundamental building block in true time delay beam-forming networks for array antennas. The network generates

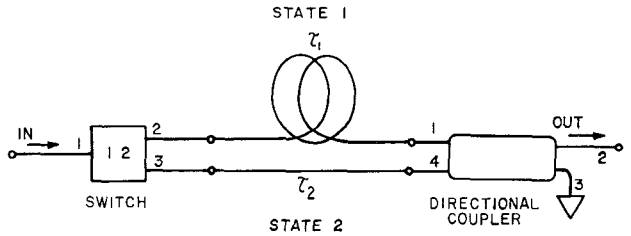


Fig. 5. Schematic of a true time delay network comprised of a $1\times2$ switch, time delay fibers, a $-3$ dB directional coupler, and a matched load at port 3 of the coupler. Circular nodes indicate elastomeric splices.

true time delays $\tau_1$ or $\tau_2$ upon application of TTL logic states to the electromechanical switch. Using the scattering matrices of the switch and directional coupler described previously, the multiport connection method [13] is applied in calculating the $S$ matrix of the network. For simplicity, the splice $S$ matrices are not used in the calculation; rather, the resulting optical $S$ parameters of the network are multiplied by $10\log|S^o_{21}|$ of each splice in each transmission path. From the multiport connection method we obtain

$$\begin{bmatrix} b_1 \\ b_6 \\ b_7 \\ b_2 \\ b_3 \\ b_4 \\ b_5 \end{bmatrix} = \left[\begin{array}{ccc|ccc|c} S^A_{11} & 0 & 0 & 0 & 0 & S^A_{13} & 0 \\ 0 & S^B_{22} & 0 & 0 & 0 & 0 & S^B_{24} \\ 0 & 0 & S^B_{33} & 0 & 0 & 0 & S^B_{34} \\ 0 & 0 & 0 & S^A_{22} & 0 & 0 & 0 \\ \hline 0 & S^B_{12} & S^B_{13} & 0 & S^B_{11} & 0 & 0 \\ S^A_{31} & 0 & 0 & 0 & 0 & S^A_{33} & 0 \\ 0 & S^B_{42} & S^B_{43} & 0 & 0 & 0 & S^B_{44} \end{array}\right] \begin{bmatrix} a_1 \\ a_6 \\ a_7 \\ a_2 \\ a_3 \\ a_4 \\ a_5 \end{bmatrix} \tag{33}$$

as the representative matrix which relates the internal and external ports of the network for components $A$ (switch) and $B$ (directional coupler). Also, for simplicity, the path lengths $l_1$ and $l_2$ of the delay lines are accounted for as $e^{j\beta(f_{RF})l_1}$ and $e^{j\beta(f_{RF})l_2}$, respectively. These are added to the appropriate coefficients of the resulting $S$ matrix, which is given for time delay $\tau_1$ as

$$S_1=\begin{bmatrix} 0.01 & 0.1485e^{j14^\circ} & 0.1414e^{-j142^\circ} \\ 0.1479e^{j10^\circ} & 0.0024e^{-j138^\circ} & 0.0025e^{-j15^\circ} \\ 0.1413e^{-j145^\circ} & 0.0025e^{-j17^\circ} & 0.0023e^{-j170^\circ} \end{bmatrix}. \tag{34}$$

Converting to a (dB, degrees) format and neglecting coefficients below $-25$ dB of optical power, we obtain

$$S_1=\begin{bmatrix} -20.0 & -8.0, 14^\circ & 0 \\ -8.3, 10^\circ & 0 & 0 \\ 0 & 0 & 0 \end{bmatrix} \tag{35}$$

which compares very well with the following measured $S$ matrix of this network, also shown in the (dB, deg) format:

$$S_1=\begin{bmatrix} -20.0 & -8.1, 12^\circ & 0 \\ -8.2, 11^\circ & 0 & 0 \\ 0 & 0 & 0 \end{bmatrix}. \tag{36}$$

The network is reciprocal to within 0.1 dB and 1° at 2.0 GHz, and true time delay behavior is verified. The multiport connection method involves multiplication of measured scattering matrices; therefore, the accuracy of this technique is dependent upon the number of components in the network and the accuracy of the measured data. Our purpose for including this method is to demonstrate that scattering matrices of fiber networks can be obtained to within a reasonable error margin during the design stage provided that the components used in the network are characterized by measured scattering matrices.

## V. Conclusion

In this paper we have introduced an optical test set that can be used with any vector network analyzer for the purpose of measuring complex-valued scattering parameters of fiber-optic components. This optical test set features a unique set of fiber-optic reflection calibration standards which include two offset shorts and a matched load. The microwave performance of these calibration standards closely resembles that of an ideal short, open, and load, and the repeatability of these standards is fairly high. The measured scattering parameters of the standards were in very close agreement with the corresponding calculated values. The error terms were calculated and a de-embedding relation was given for reflection scattering parameter measurements.

An alternate reflection de-embedding method was given that simplifies reflection calibration through the use of a frequency normalization. In this method, the frequency response tracking error term is measured from the optical test set's directional coupler, and the resulting de-embedded data were found to be in very close agreement with values obtained using the offset shorts and matched load calibration.

A fiber-optic thru calibration standard is used for transmission scattering parameter calibration and de-embedding is performed automatically by the network analyzer. The measurement uncertainty of the optical test set was determined for transmission and reflection measurements, based on connection repeatability, accuracy of reflection error correction terms, and measured data from known attenuators and cleaved fiber. From these results we found the magnitude uncertainty to be $\pm 0.15$ dB in optical power, $\pm 1°$ phase uncertainty for transmission, and $\pm 2°$ phase uncertainty for reflection. The dynamic range was 47.4 dB for transmission and 40.9 dB for reflection, again in dB of optical power. The resolution of the test set was limited to that of the network analyzer.

In addition to the optical test set, definitions were given for microwave scattering parameters of fiber-optic components in terms of optical power wave variables and the electrical power ratios displayed by the network analyzer. *OSWR* was defined in terms of the RF-modulated transmitted and reflected waves, and measured *S*-matrices were shown for a fiber-optic directional coupler, a $1 \times 2$ switch, and a true time delay network composed of these components.

## References


[1] T. R. Joseph and W. E. Stephens, "The fiber optics link to future systems," *Microwave Syst. News*, June 1987.

[2] P. G. Sheehan and J. R. Forrest, "The use of optical techniques for beamforming in phased arrays," *SPIE*, vol. 477, *Optical Technology for Microwave Applications*, 1984.

[3] L. Cardone, "Ultra-wideband microwave beamforming technique," *Microwave J.*, Apr. 1985.

[4] P. R. Herczfeld and A. S. Daryoush, "Fiber optic feed networks for large aperture phased array antennas," *Microwave J.*, Aug. 1987.

[5] J. J. Pan, "Fiber optics and opto-electronics for radar and electronic-warfare applications," *Microwave Syst. News*, Oct. 1987.

[6] K. Bowe, "Characterization of high-speed optical components," *Microwave Syst. News*, Dec. 1987.

[7] *Technical Data: HP8702A Lightwave Component Analyzer*, Hewlett Packard, 1988.

[8] G. Keiser, *Optical Fiber Communications*. New York: McGraw-Hill, 1983.

[9] L. B. Jeunhomme, *Single-Mode Fiber Optics, Principles and Applications*. New York: Marcel Dekker, 1983.

[10] C. G. Montgomery, R. H. Dicke, and E. M. Purcell, *Principles of Microwave Circuits*. New York: McGraw-Hill, 1948.

[11] A. Yariv, *Optical Electronics*. New York: Holt, Rinehart and Winston, 1985.

[12] E. L. Dereniak and D. G. Crowe, *Optical Radiation Detectors*. New York: Wiley, 1984.

[13] K. C. Gupta, R. Garg, and R. Chadha, *Computer-Aided Design of Microwave Circuits*. Dedham, MA: Artech House, 1981.



**David D. Curtis** (S'83–M'87) was born in Hartford, CT, on March 1, 1961. He received the B.S. and M.S. degrees in electrical engineering from Northeastern University, Boston, MA, in 1986 and 1989, respectively. The subject of his master's thesis was phased array antenna beam forming using fiber-optic true time delays. During his graduate studies, he held an instructional assistantship in electrical engineering and was employed part-time at the Rome Air Development Center, Hanscom Air Force Base, MA, where he performed his thesis research.

He has been employed full-time at RADC since June, 1987. His current research is in optical beam-forming techniques for array antennas.

Mr. Curtis is a member of Tau Beta Pi and Eta Kappa Nu.



**Elizabeth E. Ames** (S'70–M'81) received the B.S., M.S., and Ph.D. degrees in electrical engineering from Northeastern University, where she performed research on high-voltage plasma discharges in vacuum.

Since then, she has been with Northeastern University as an Assistant Professor in the Electrical and Computer Engineering Department, and is currently a Senior Scientist with the Center for Electromagnetics Research, where she is directing a research project on optical feed networks for phased array antennas.